SAND2017-0228R

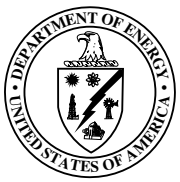

Sandia National Laboratories

Operated for the U.S. Department of Energy by

Sandia Corporation

Albuquerque, New Mexico 87185

date: January 5, 2017

to: Distribution

from: Edmundo Corona, Org. 1554
Bo Song, Org. 1528

subject: Wave transmission through silicone foam pads in a compression Kolsky bar apparatus. Comparison between simulations and measurements.

Abstract

This memo concerns the transmission of mechanical signals through silicone foam pads in a compression Kolsky bar set-up. The results of numerical simulations for four levels of pad pre-compression and two striker velocities were compared directly to test measurements to assess the fidelity of the simulations. The finite element model simulated the Kolsky tests in their entirety and used the hyperelastic 'hyperfoam' model for the silicone foam pads. Calibration of the hyperfoam model was deduced from quasi-static compression data. It was necessary, however, to augment the material model by adding stiffness proportional damping in order to generate results that resembled the experimental measurements. Based on the results presented here, it is important to account for the dynamic behavior of polymeric foams in numerical simulations that involve high loading rates.

Introduction

Of interest here is the numerical simulation of the transmission of mechanical signals through pre-compressed silicone foam pad specimens under impact conditions. Figure 1 shows an image of the structure of cellular silicone. It essentially is a silicone block where a large

number of voids have been introduced by the manufacturing process. The objective of the study was to determine how well a hyperelastic model of cellular silicone could reproduce the experimental observations of the amplitude and time history of the pulse transmitted by the foam pad from the incident to the transmission bar of a Kolsky bar compression apparatus.

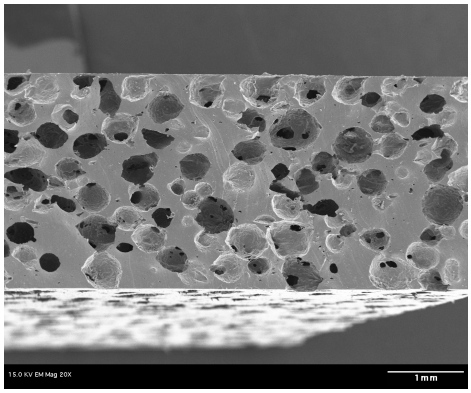

Figure 1. Image showing the structure of cellular silicone.

Figure 2(a) shows a schematic of the Kolsky bar set-up. The circular cylindrical silicone foam sample is sandwiched between the incident (I) and transmission (T) steel bars. It has diameter of one inch, which is equal to the diameter of the bars and a length of 0.210 in. A confinement sleeve fits over the bars and the specimen as shown. Static pre-compression is achieved by pushing the right side of the transmission bar towards the left with a hydraulic actuator (not shown). In the model, this is represented by the pressure P. A fixed reaction plate holds the incident bar to react the applied load using a second plate that fits between the incident bar and the reaction plate, as shown. The reaction plate has a hole to allow the striker bar, moving with speed V_1, to pass through and strike the plate in contact with the incident bar. The striker is a tapered tungsten carbide bar with the dimensions given in Fig. 2(b). The test instrumentation relevant to this study consists of strain gages and associated circuitry that measure the strain induced in the bars by the passing stress pulses at location 1 in the incident bar and at location 2 in the transmission bar as seen in Fig. 2(a). The strain signals are recorded using a high-speed digital oscilloscope.

The calibration of the hyperelastic model was based on a single confined compression test of a specimen assumed to be of the same material as the samples tested in the Kolsky bar. The quasi-static test sample had nominal density $\rho = 36$ lb/ft^3, prosity of $p = 47\%$ and thickness $h = 0.125$ in. The test was one of four conducted by Wai-Yang Lu (Org. 08343) as reported by Hinnerichs (2015). The measured engineering stress-strain curve is shown by the line with circular symbols in Fig. 3.

Hinnerichs also conducted a fit of the hyperelastic 'hyperfoam' model to the compression data shown. Brief descriptions of the hyperfoam model are provided in Section 22.5.2 of Dassault Systemes (2014) and Section 5.2.22 of Sierra Solid Mechanics Team (2016). Hinnerich's fit of the hyperfoam model was conducted in Abaqus/Standard (Dassault Systemes, 2014) using the provided fitting methods. Whereas a variety of material test conditions are suggested

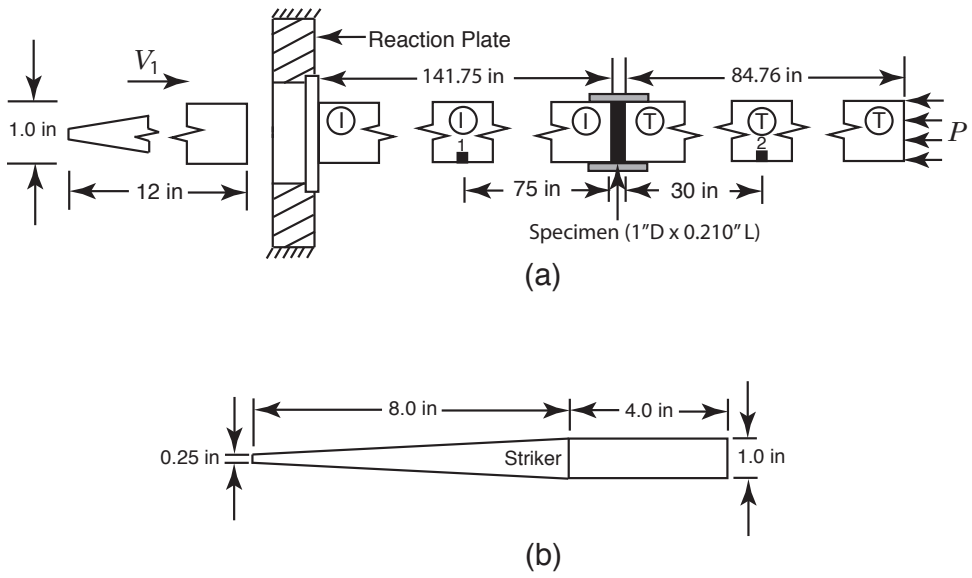

Figure 2. Diagram of the experimental apparatus.

in Dassault Systemes (2014) to fit the hyperfoam model, the work conducted here only considered the confined compression data. This might be considered sufficient in this case since the loading in the Kolsky bar tests is also confined compression, although at a much higher rate. The parameters of Hinnerich's fit were used in an Abaqus/Standard one-element axisymmetric model that simulated confined compression. The results of the simulation are also shown in Fig. 3 and show reasonable agreement with the test data.

Finite Element Model of Kolsky Bar Test

An axisymmetric finite element model of the Kolsky bar tests was constructed based on the dimensions shown in Fig. 2, and the simulations were conducted using Abaqus. Most of the elements are used to model the straight steel incident and transmission bars. The two regions that contain other geometric entities are the location where the striker impacts the incident bar shown in Fig. 4(a), and the location of the specimen shown in Fig. 4(b). These figures also show the mesh of the model. The standard mesh has four elements through the radius of the steel bars, whereas the specimen has 25 elements through the radius. Most elements had nearly unit aspect ratios. The specimen had to be meshed relatively finely to capture the axial propagation of strain waves. Variations of the element size in the specimen from 12 to 100 through the radius had minor effects in the calculated transmitted signal as will be shown. All elements in the model were four-node axisymmetric elements with reduced integration, Abaqus CAX4R. The interaction between the various components that came in contact during the simulations were simulated using a penalty contact formulation. The penalty parameter had to be scaled 100 times over the default value in order to minimize interpenetration at the bar/specimen interface. This caused a reduction of the critical time step size of the explicit solution scheme. Other than for scaling the penalty parameter, all

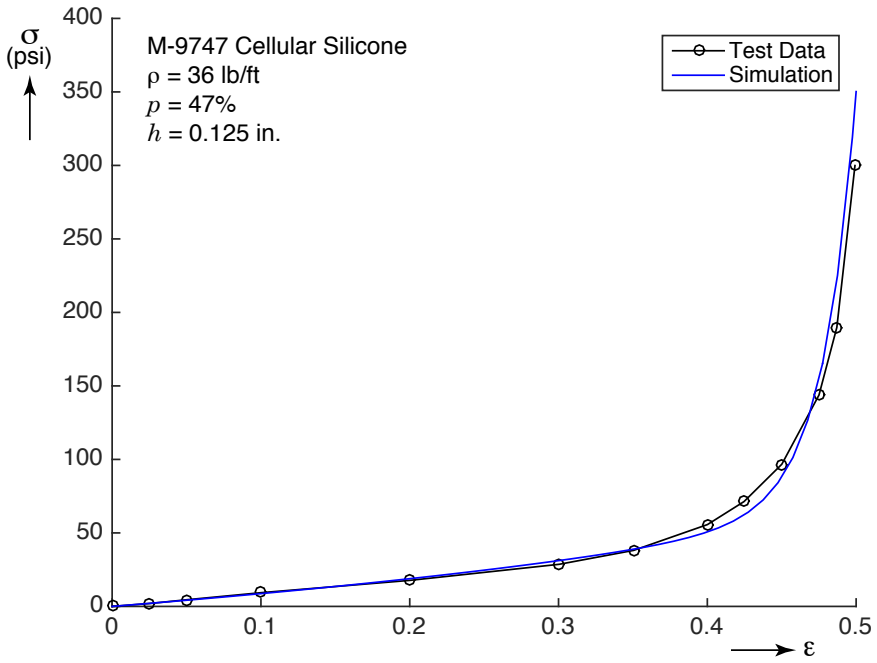

Figure 3. Comparison of the quasi-static compressive stress strain curves of a sample and the results of a one-element analysis.

other numerical parameters of the model were kept at their default values.

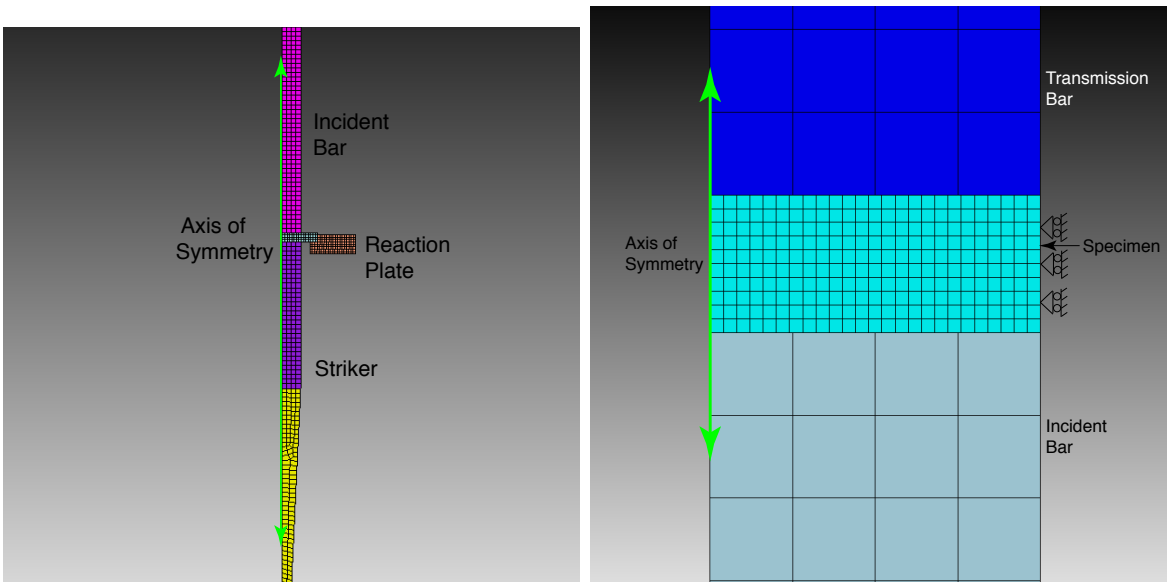

Figure 4. Geometrically non-uniform regions in the model. (a) Striker impact location and (b) specimen location.

All the simulations that involved pre-compression of the specimen were run in two steps. The first involved quasi-static compression of the specimen to the desired value and was conducted using Abaqus/Standard by prescribing the pressure P to the right end of the transmission bar. The value of the pressure was determined iteratively until the desired pre-compression in the specimen was achieved. The state of the model was then handed to Abaqus/Explicit, which was used to simulate the dynamic part of the test. The tests with no pre-compression were conducted with a slightly modified model that did not contain the reaction plate.

Results

Experimental

The experiments were conducted in the Experimental Impact Mechanics Lab in Building 860 for four pre-compression levels and two striker speeds. Figure 5(a) and (b) show the strain signals measured as functions of time (t, shifted so $t = 0$ matches the start of the numerical simulations; impact between the striker and the Kolsky apparatus occurs at $t = 0.023$ ms) at location 1 in the incident bar and 2 in the transmission bar (see Fig. 2(a) for the locations of 1 and 2). These results are for the slower striker speed. The strain signals in the incident bar are denoted by ε_i in Fig. 5(a). Four signals are shown in the figure corresponding to pre-compression engineering strains of $\varepsilon_p = 0$, 13%, 23.3% and 33.5%. Clearly, the value of ε_p has essentially no effect on the recorded traces of the incident and reflected pulses. The first negative strain pulse, which starts at $t = 0.36$ ms, corresponds to the incident pulse. The fact that the four signals are virtually identical, indicates nearly consistent striker speeds. The amplitude of the strain signal is 1 mε. Based on the numerical model, this strain amplitude occurs when the striker velocity is 215 in/s. The positive strain pulses correspond to the signal reflected at the bar/specimen interface and have essentially the same amplitude and shape as the incident signals. This demonstrates that the impedance of the specimen is negligible, and the incident pulse is reflected essentially at a free end. The reflected pulse has more oscillations in the falling side likely due to the effects of dispersion in the incident bar. The second negative pulse at $t = 1.85$ ms occurs after the pulse reflects at the impact end and is not significant to the results presented here.

Figure 5(b) shows the transmitted strain traces, ε_t, measured at point 2 in the transmission bar. They all start at nearly the same time, approximately 1 ms. Note that the amplitudes of the traces are between two and three orders of magnitude smaller than those in the incident bar, and that the value of ε_p has a large effect on the characteristics of the transmitted strain signal. In particular, the amplitude of the pulses increases with the value of ε_p. Also note that the time required for the pulse to travel from point 2 to the end of the transmission bar and back to point 2 is 0.58 ms, so the arrival of that reflected wave occurs at approximately 1.6 ms. The positive-going spikes seen at approximately this time for all traces represent the arrival of these signals. Therefore, the time of interest in this work is between zero and 1.6 ms.

Figure 6 shows the results obtained for the second set of tests, with a faster striker velocity.

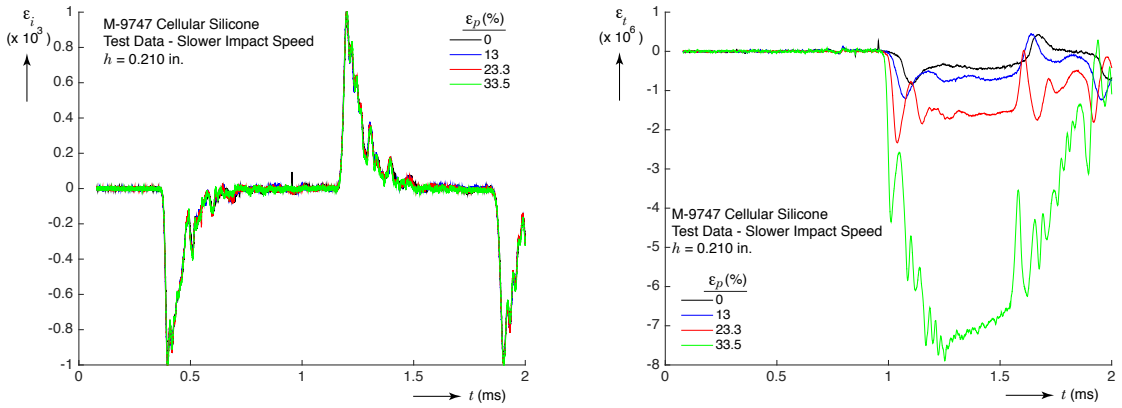

Figure 5. Experimentally measured strain signals as functions of time for the slower impact speed. (a) At point 1, in the incident bar and (b) at point 2, in the transmission bar.

As seen previously, the incident pulses in Fig. 6(a) are essentially the same for all tests, showing that all had similar striker velocity. The peak incident strain amplitude was a little over 2 mε, corresponding to a striker velocity of 487 in/s based on analysis results. The reflected pulses, however, are somewhat different between the tests, indicating that the impedance of the specimen is not negligible in this case. The higher impedance may be due, at least in part, to the high compression developed in the sample that causes significant stiffening of its stress-strain response, particularly after applying significant pre-compression.

Figures 6(b) and (c) show the strain signals recorded in the transmission bar for 0, 13%, and 23.3, 33.5% strain pre-compression respectively. They are plotted in different figures in order to adjust the scales to ease the presentation since their amplitudes cover a range of almost three orders of magnitude. The case with no pre-compression has similar shape as that obtained for the slower impact speed, except it shows more prominent oscillations and its amplitude is somewhat higher. The case with 13% pre-compression has much higher pulse amplitude, even higher than the one with 33.5% pre-compression and slower impact speed. The shape of the pulse actually resembles more the previous case with 33.5% pre-compression than the one with with 13% pre-compression. Recall that the signals after 1.6 ms are altered by the arrival of the pulse reflected from the end of the transmission bar. The responses obtained for 23.3 and 33.5% pre-compression have significantly different character from the others. In both cases, the transmitted signals display sharp peaks with much larger amplitudes, up to 800 $\mu\varepsilon$ in the case with $\varepsilon_p = 33.5\%$, but relatively short durations, followed by a gradual decay before the pulse reflected from the end of the bar arrives at the strain gage location.

In summary, the experimental results show that the transmission of pulses through the cellular silicone pads are complex events and that the signals transmitted depend on both the level of pre-compression in the pad as well as on the striker velocity. Not only are the

transmitted signal amplitudes significantly affected by these parameters, but also their time histories.

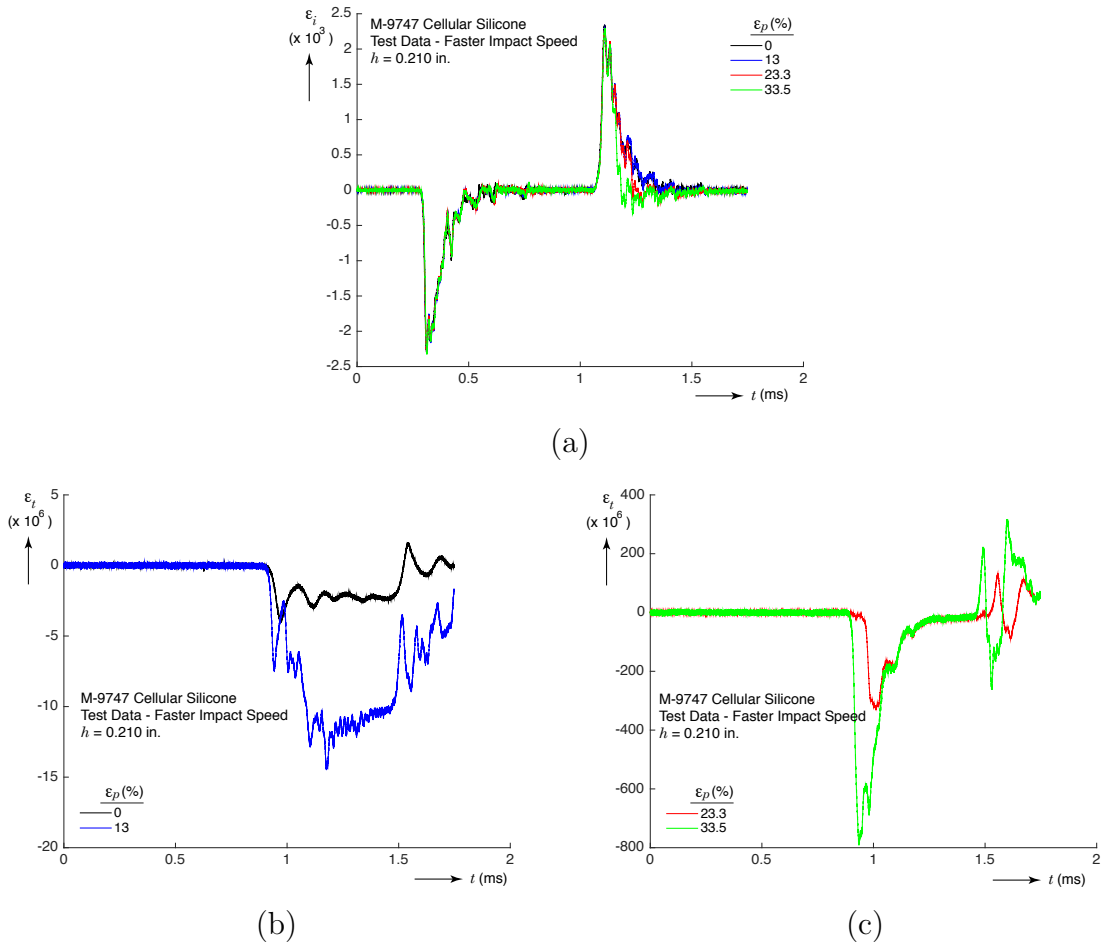

Figure 6. Experimentally measured strain signals as functions of time for the faster impact speed. (a) At point 1, in the incident bar and (b) at point 2, in the transmission bar.

Numerical

This section presents a comparison of the finite element model results against the test measurements. As indicated earlier, the main criterion to assess the numerical results is the amplitude and shape of the pulses recorded in the transmission bar of the Kolsky bar set-up. Comparisons of the reflected pulses will also be presented for completeness although these comparisons are not as significant since the reflected pulse in most cases was essentially like the incident pulse, but with opposite sign. In other words it was not significantly influenced by the specimen.

Slower striker speed

The first case considered is the one with the slower striker speed and no pre-compression ($V_1 = 215$ in/s, $\varepsilon_p = 0$). Figure 7 shows the results obtained. Note in Fig. 7(a) that the measured incident pulse is predicted very well by the simulation, thus indicating that impact between the striker and incident bars is modeled well. Therefore, the pulse applied to the specimen in the simulation should be very similar to that applied in the tests. The predicted transmitted pulse, in the other hand, is significantly different from the measured one. The predicted pulse is slightly delayed, it displays a significantly larger strain values and much more pronounced oscillations.

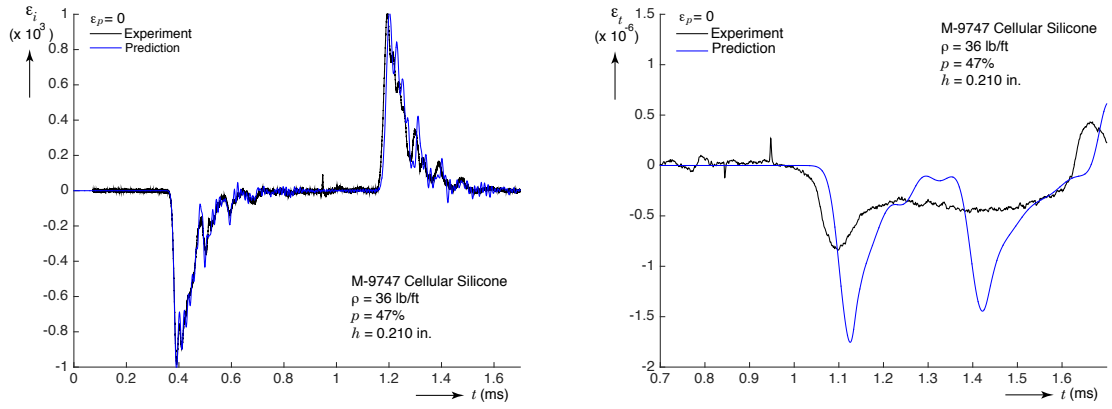

(a) (b)

Figure 7. Comparison of predicted and experimental results for $V_1 = 215$ in/s and $\varepsilon_p = 0$. (a) Incident and reflected strain pulses and (b) transmitted strain pulses.

The predicted oscillations in the strain signal, combined with the polymeric character of the specimen gave rise to the speculation that some degree of damping should be added to the simulations to see if the comparison between measurement and simulation could be improved. To assess this, Rayleigh damping (Dassault Systemes, 2014: Section 26.1.1) was added to the specimen. Rayleigh damping has mass proportional and stiffness proportional components. Numerical simulations indicated that adding the stiffness proportional component produced the most desirable results. Therefore, mass proportional damping was not included in the

model. Figure 8 shows how the measured reflected and transmitted pulses were affected by various values of the stiffness proportional damping parameter (β). Clearly, the effect on the reflected pulse in Fig. 8(a) is negligible. The transmitted pulse, however, is significantly affected by the chosen value. As β increases, the predicted pulse arrives earlier, the amplitude of the strain signal decreases and so does the oscillatory response observed in the undamped case. Based on the comparison presented, it seems that using a value of $\beta = 0.00005$ produces a pulse that matches the measurements relatively well.

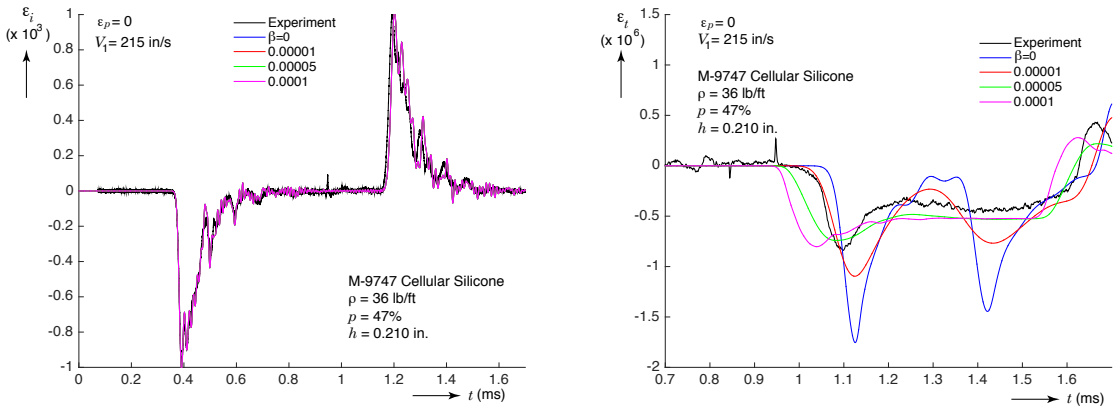

(a) (b)

Figure 8. Comparison of predicted and experimental results for $V_1 = 215$ in/s and $\varepsilon_p = 0$ with various values of stiffness proportional damping β applied to the specimen material. (a) Incident and reflected strain pulses and (b) transmitted strain pulses.

The preceding results were all conducted with the standard mesh described previously. At this point it is useful to consider the effects of the finite element mesh in the specimen on the results. Figure 9(a) shows the effect of varying the element size (h_e) on the transmitted pulse when the specimen material does not include Rayleigh damping. Clearly the results are somewhat mesh dependent. Finer meshes predict sharper and larger strain peaks and resolve higher harmonics. For the rest of the results presented in this memo, $h_e = 0.02$ inches will be used. This gives 25 elements through the specimen radius and 10 elements along its length (the standard mesh). Figure 9(b) shows that when the material includes damping, the standard mesh adopted and the finest mesh considered give essentially the same result, indicating that damping reduces the mesh sensitivity of the transmitted pulse.

Once the damping coefficient β and the element size have been chosen, they will remain fixed for the rest of the cases considered. The work included assessing the effect of element size under other values of ε_p and V_1, but the conclusions remained unchanged. The results of calculations with $\beta = 0$ and 0.00005 will be compared to the measurements from the experiments for the rest of this memo.

The results for the slower striker speed and progressively increasing pre-compression values will be shown first. Figure 10 shows the results for $\varepsilon_p = 13\%$. Again, the reflected pulse is

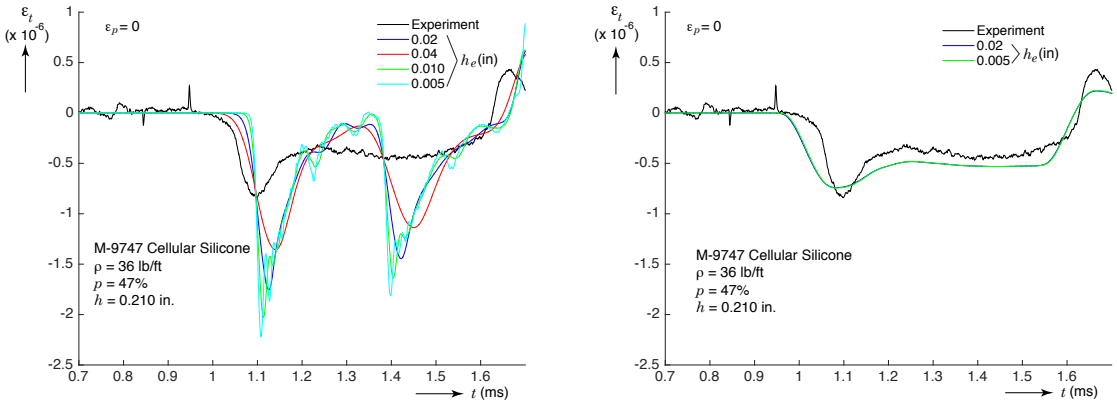

Figure 9. Effect of element size on the prediction of the transmitted pulse. (a) Without damping and (b) with damping.

unremarkable, with the predictions matching the measurements well and showing no effect to the value of β. The transmitted pulse shows similar conclusions as before: including damping with $\beta = 0.00005$ makes the predicted signal resemble the measurements.

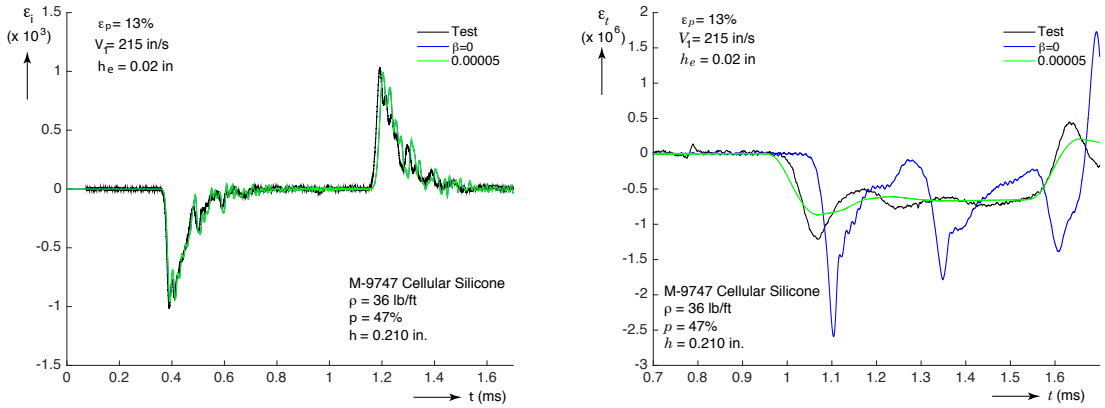

Figure 10. Comparison of predicted and experimental results for $V_1 = 215$ in/s and $\varepsilon_p = 13\%$. (a) Incident and reflected strain pulses and (b) transmitted strain pulses.

Figure 11 shows the results when $\varepsilon_p = 23.3\%$. In this case the predictions of the transmitted pulse underpredict the measured amplitude by about 50%, but the results with damping qualitatively resemble the shape of the measured curve better.

Figure 12 shows results for $\varepsilon_p = 33.5\%$. This case is different in several respects from the previous three. First, note that the undamped prediction is not far from the test measurements. Although it rings more and at a higher frequency than in the previous cases, its mean value

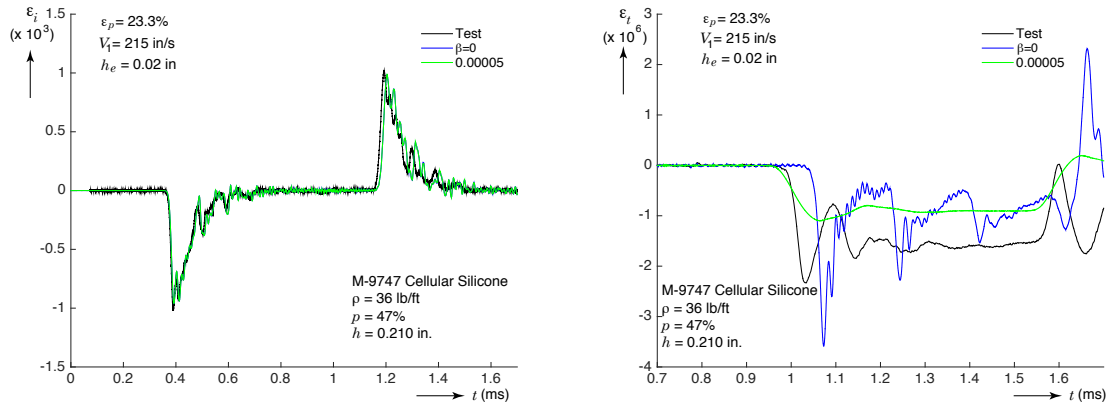

(a) (b)

Figure 11. Comparison of predicted and experimental results for $V_1 = 215$ in/s and $\varepsilon_p = 23.3\%$. (a) Incident and reflected strain pulses and (b) transmitted strain pulses.

is close to the test results. This is most likely due to the fact that 33.5% pre-compression puts the material at a strain near to the point where significant stiffening occurs, as can be seen in the stress-strain response shown in Fig. 3. Regarding the predictions with damping, note that, in addition to reducing the amplitude of oscillations, it also causes the predicted pulse signal to have higher amplitude than the undamped prediction over a significant period of time.

Further calculations with this value of pre-compression indicated that the predictions are more sensitive to small variations in the pre-compression amount and of the striker speed than when the pre-compression is smaller. This is likely due to the fact that the regime of strains active during wave transmission through the specimen lies more in the highly nonlinearly stiffening part of the curve in Fig. 3 than the cases with smaller pre-compression.

Faster Striker Speed

The next four cases considered correspond to the same values of pre-compression examined before, but now for the higher striker speed, in the vicinity of 487 in/s. The comparison between predictions and measurements for the case with no pre-compression is shown in Fig. 13. Whereas the model accurately predicts the incident and transmitted pulses in Fig. 13(a), the more interesting part of the comparison is between the transmitted pulses in Fig. 13(b). Here the predictions with $\beta = 0$ display more amplitude variation than the measured results, while the damped case shows a flatter response that reduces the amplitude of the first negative-going peak significantly. Perhaps a lower value of damping would have matched the test results better, but the results obtained with $\beta = 0.00005$ still resemble the measurements in an acceptable manner.

Figure 14 shows results for $\varepsilon_p = 13\%$. In this case the predictions underestimate the amplitude of the transmitted pulse by about 50%. The predicted responses with and without

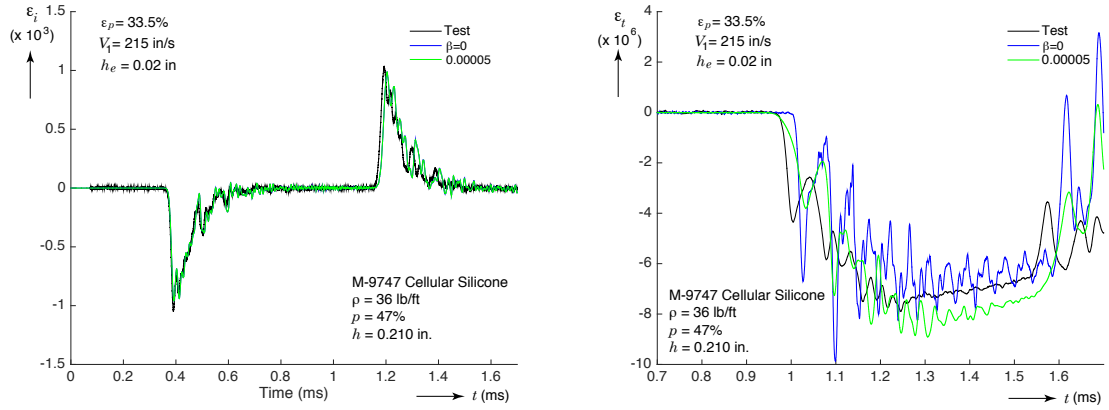

(a) (b)

Figure 12. Comparison of predicted and experimental results for $V_1 = 215$ in/s and $\varepsilon_p = 33.5\%$. (a) Incident and reflected strain pulses and (b) transmitted strain pulses.

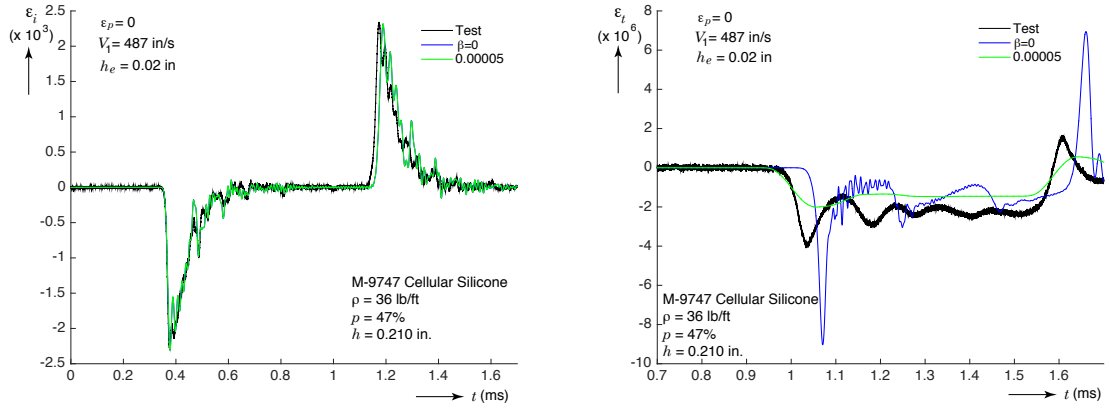

(a) (b)

Figure 13. Comparison of predicted and experimental results for $V_1 = 487$ in/s and $\varepsilon_p = 0$. (a) Incident and reflected strain pulses and (b) transmitted strain pulses.

damping are somewhat similar, with the damped response showing smaller amplitude oscillations, more in line with the measured response.

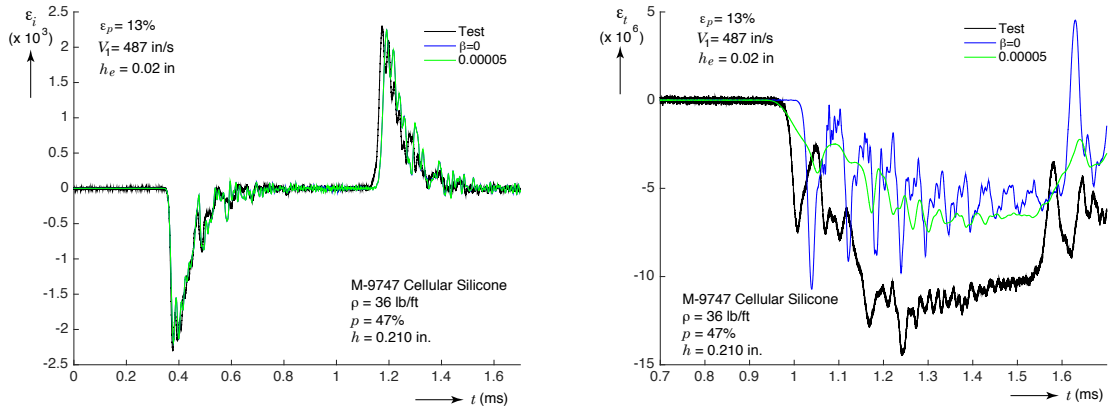

(a) (b)

Figure 14. Comparison of predicted and experimental results for $V_1 = 487$ in/s and $\varepsilon_p = 13\%$. (a) Incident and reflected strain pulses and (b) transmitted strain pulses.

Starting with the pre-compression value of 23.3%, the amplitude of the measured transmission signals jump by one order of magnitude compared to the cases with lower pre-compression as shown in Fig. 6. This indicates that a different regime of the material response has been entered. Note also the differences in the reflected pulses in the same figure. The comparisons between simulation and measurement for the case with $\varepsilon_p = 23.3\%$ are shown in Fig. 15. The difference between the response of the undamped model and the test measurements shown in Fig. 15 is now immense, about one order of magnitude in the amplitude at the front of the pulse. Adding damping with $\beta = 0.00005$ gives a response that, while still significantly short in amplitude with respect to the test data, is at least on track to represent the measured response.

The last case considered is for pre-compression of 33.5% and is shown in Fig. 16. Looking first at the transmitted pulse in Fig. 16(b), reinforces the observations in the previous case. The undamped model significantly underestimates the amplitude of the transmitted pulse, while the damped case has reasonable agreement with the measurements in this case. Looking at the reflected pulse next in Fig. 16(a) the addition of damping has a discernible effect on the reflected pulse.

Conclusions

This memo presented results of a first attempt to model the transmission of mechanical signals through silicone foam pads in a Kolsky bar test set-up. The simulations involved finite element models of the Kolsky set up for four levels of pad pre-compression and two striker bar velocities. The results presented concentrated on the signal transmitted by the

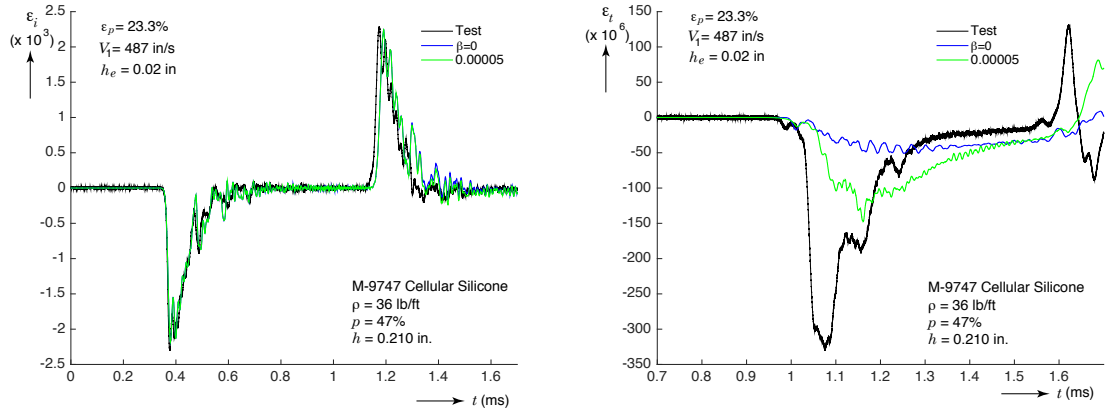

(a) (b)

Figure 15. Comparison of predicted and experimental results for $V_1 = 487$ in/s and $\varepsilon_p = 23.3\%$. (a) Incident and reflected strain pulses and (b) transmitted strain pulses.

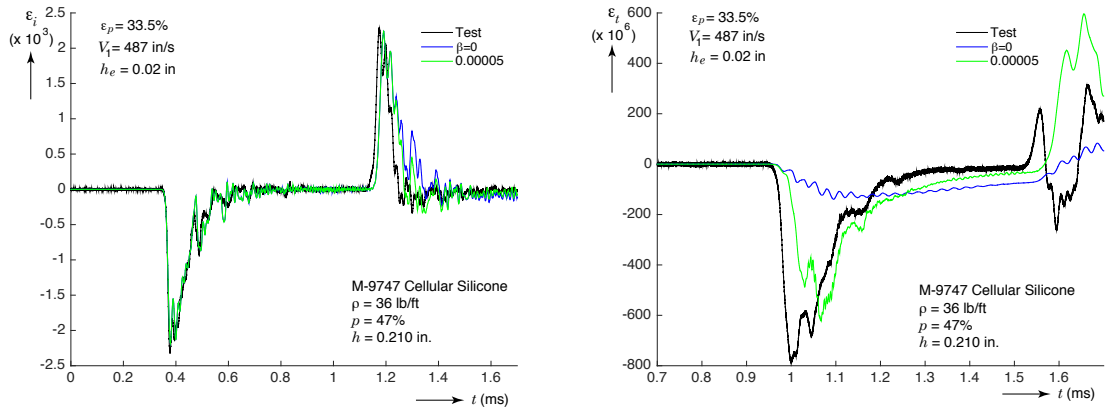

(a) (b)

Figure 16. Comparison of predicted and experimental results for $V_1 = 487$ in/s and $\varepsilon_p = 33.5\%$. (a) Incident and reflected strain pulses and (b) transmitted strain pulses.

pad to the transmission bar of the test set-up. The deformation of the pads during pulse transmission will be addressed later in FY17.

The principal conclusions of the work presented here can be listed as follows:

- The hyperfoam model as caibrated by Hinnerichs (2015) matches the non-linear, hardening stress-strain response measured quasi-statically well.
- The dynamic response of the silicone foam pads is relatively complex. This can be attributed in part due to the nonlinearity of its quasi-static stress-strain curve and also to a time dependence that was addressed here through a simple damping model.
- The material model utilized here is relatively simplistic, with a stiffness proportional damping model attached to a hyperelastic model.
  - The hyperelastic component of the model was well behaved in all but one case. The model crashed while studying the effect of element size under the most severe loading conditions (highest pre-compression and striker speed), with the smallest element considered and no damping.
  - Stiffness proportional damping was added in an ad-hoc manner to investigate its effect. The results showed that including damping was essential to make the predictions resemble the test results.
- Clearly the work presented here constitutes a first effort to model the dynamic mechanical signal transmission through silicone foam pads. More work to explore other material models and their associated calibrations is necessary to improve the capabilities of our computational simulations to address similar classes of problems.

Finally, based on the results presented here, it is important to account for the dynamic behavior of polymeric foams in numerical simulations that involve high loading rates since it can be significantly different from the behavior suggested by test data obtained under quasi-static conditions.

References

Dassault Systemes (2014). Abaqus 6.14 analysis user's guide.

Hinnerichs, T. (2015). Memo to distribution. June 29, 2015.

Sierra Solid Mechanics Team (2016). Sierra/SolidMechanics 4.42 user's guide. Sandia National Laboratories report.

Acknowledgments

Thanks to Chris Hammeter for providing the image shown in Fig. 1.

Sandia National Laboratories is a multi-mission laboratory managed and operated by Sandia Corporation, a wholly owned subsidiary of Lockheed Martin Corporation, for the U.S. Department of Energy's National Nuclear Security Administration under contract DE-AC04-94AL85000.

Internal Distribution:

Dennis Croessmann	1520
Darrick Jones	1528
Sharlotte Kramer	1528
Brett Sanborn	1528
Jim Redmond	1550
Jim Bean	1554
Nicole Breivik	1554
Eliot Fang	1554
Chris Hammetter	1554
Kevin Long	1554
Brian Lester	1554
Benjamin Reedlunn	1554
William Scherzinger	1554
Michael Wong	1554
Steve Attaway	1555